Clim. Past Discuss., 9, 3953–3991, 2013
www.clim-past-discuss.net/9/3953/2013/
doi:10.5194/cpd-9-3953-2013

Climate of the Past Discussions
Open Access

Investigating the consistency between proxies and between proxies and models using data assimilation: a mid-Holocene case study

A. Mairesse[1], **H. Goosse**[1], **P. Mathiot**[1,*], **H. Wanner**[2], **and S. Dubinkina**[1]

[1]Université catholique de Louvain, Earth and Life Institute, Georges Lemaître Centre for Earth and Climate Research, Place Louis Pasteur, 3, 1348 Louvain-la-Neuve, Belgium
[2]Institute of Geography and Oeschger Centre for Climate Change Research, University of Bern, Bern, Switzerland
[*]now at: British Antarctic Survey, Natural Environment Research Council, Cambridge, UK

Received: 20 June 2013 – Accepted: 2 July 2013 – Published: 12 July 2013

Correspondence to: A. Mairesse (aurelien.mairesse@uclouvain.be)

Published by Copernicus Publications on behalf of the European Geosciences Union.

Abstract

The mid-Holocene (6 thousand years before present) is a key period to study the consistency between model results and proxy data as it corresponds to a standard test for models and a reasonable number of proxy records are available. Taking advantage of this relatively large amount of information, we have first compared a compilation of 50 air and sea surface temperature reconstructions with the results of three simulations performed with general circulation models and one carried out with LOVECLIM, a model of intermediate complexity. The conclusions derived from this analysis confirm that models and data agree on the large-scale spatial pattern but underestimate the magnitude of some observed changes and that large discrepancies are observed at the local scale. To further investigate the origin of those inconsistencies, we have constrained LOVECLIM to follow the signal recorded by the proxies selected in the compilation using a data assimilation method based on a particle filter. In one simulation, all the 50 proxies are used while in the other two, only the continental or oceanic proxies constrains the model results. This assimilation improves the consistency between model results and the reconstructions. In particular, this is achieved in a robust way in all the experiments through a strengthening of the westerlies at mid-latitude that warms up the Northern Europe. Furthermore, the comparison of the LOVECLIM simulations with and without data assimilation has also objectively identified 16 proxies whose reconstructed signal is either incompatible with the one recorded by some other proxies or with model physics.

1 Introduction

The Holocene, our current interglacial, has been the subject of a large number of studies based on reconstructions derived from proxy records (e.g., Bartlein et al., 2011; Davis et al., 2003; Leduc et al., 2010; Marcott et al., 2013; Viau and Gajewski, 2009; Vinther et al., 2009) and on simulations performed with climate models of various com-

CPD
9, 3953–3991, 2013

plexities (e.g., Braconnot et al., 2007a,b; Claussen et al., 1999; Crucifix, 2008; Renssen et al., 2012; Zhao et al., 2005). The two approaches are complementary (Mock, 2007) as the information inferred from the proxies often serves to validate the climate model results (Braconnot et al., 2012) while the models allow the exploration of the physical processes responsible for the recorded climatic changes.

In particular, the mid-Holocene, corresponding to 6 ky BP (thousand years before present), is a standard period in the Paleoclimate Modelling Intercomparison Project (PMIP) for which boundary conditions have been specified to facilitate the comparison between models results and with reconstructions. One of the most robust conclusions of those model studies is that the summer of the mid to high latitudes of the Northern Hemisphere is warmer during the mid-Holocene compared to the pre-industrial conditions (Braconnot et al., 2007a). This is consistent with the trends of the pollen-based reconstructions of Bartlein et al. (2011) and Davis et al. (2003) for Northern Europe and with several other proxy records (e.g., Andreev et al., 2003; Clegg et al., 2010; Marcott et al., 2013; Seppä and Birks, 2002, 2001; Vinther et al., 2009).

The model-data comparisons have nonetheless underlined some major differences between reconstructions and simulation results. Brewer et al. (2007b) have highlighted that PMIP2 models are able to capture the large-scale surface temperature patterns over Europe reconstructed from pollen records, but they tend to underestimate the magnitude of the observed changes, which is also in agreement with the conclusion of Braconnot et al. (2007a). Lohmann et al. (2012) have found similar results when analyzing the trends of annual mean sea surface temperature of the last 6000 yr obtained from alkenone data: the large-scale spatial pattern derived from the proxies is consistent with the ones of models, while the latter underestimate the magnitude of the changes.

Moreover, Lohmann et al. (2012) have not been able to find any link between modeled sea surface temperatures and reconstructed ones based on Mg/Ca proxies. Furthermore, Hargreaves et al. (2013) have shown that, at the local scale, models fail to reproduce the difference between mid-Holocene and pre-industrial temperature recon-

CPD
9, 3953–3991, 2013

structed by Leduc et al. (2010) for sea surface temperature and Bartlein et al. (2011) for land temperature.

Our goal here is to further investigate the origin of those inconstancies between model results and reconstructions using simulations with data assimilation. Data assimilation evaluates which state of the system is the most consistent with all the sources of information, derived here from a climate model, the forcing and the proxy records. By performing different experiments, driven by different subsets of proxies, we plan to identify the ones that are compatible with model physics, the ones that are not, and those that are incompatible with other proxy records.

We focus on the mid-Holocene as this is a well-documented period. LOVECLIM1.2 (Goosse et al., 2010), a three-dimensional Earth Model of Intermediate Complexity, is constrained to follow a compilation of 50 air and sea surface temperature reconstructions located in the Northern Hemisphere by means of a particle filter with resampling (Dubinkina et al., 2011). These simulations with data assimilation will be compared with a simulation performed with LOVECLIM without data assimilation and with three GCMs (General Circulation Models) simulations following the PMIP3-CMIP5 framework (Paleoclimate Models Intercomparison Project phase 3 – Coupled Model Inter-comparison Project phase 5) in order to assess the dependance of model-data differences on the model selected.

The methodology is presented in Sect. 2, including a description of LOVECLIM, the data assimilation method, the proxy dataset and the experimental design. This is followed by the analysis and the discussion of the model results without and with data assimilation in Sect. 3. The conclusions are drawn in the Sect. 4.

CPD
9, 3953–3991, 2013

2 Methodology

2.1 Description of LOVECLIM1.2

LOVECLIM1.2 is based on a simplified representation of the dynamics of the climate system and has a coarse horizontal and vertical resolution which enables low computational requirements. Therefore, the large ensembles of simulations required by data assimilation can be performed at a reasonable cost. This model includes three main components named ECBilt2, CLIO3 and VECODE, which represent the development of the atmosphere, the ocean and the vegetation, respectively. ECBilt2 is a spectral T21 (corresponding to about 5.625° in latitude and longitude) global 3-level quasi-geostrophic model (Opsteegh et al., 1998). CLIO3 is an ocean general circulation model coupled to a comprehensive sea-ice model (Goosse and Fichefet, 1999). It has a horizontal resolution of 3° × 3° and 20 unequally spaced vertical levels ranging from 10 m near surface to 500 m at 5500 m depth. VECODE is the continental biosphere component that describes the distribution of trees, grass and desert at the same resolution as ECBilt2 (Brovkin et al., 1997). For a complete description of LOVECLIM1.2, please refer to Goosse et al. (2010).

2.2 Assimilation method

The particle filter with resampling applied here is identical to the one described in Dubinkina et al. (2011) and used in several recent studies (e.g., Goosse et al., 2012; Mathiot et al., 2013). An ensemble of 96 simulations, also referred to as particles or ensemble members, is first initiated from slightly different states obtained by perturbing the surface temperature of an equilibrium experiment under the same conditions as the simulation without data assimilation (Dubinkina and Goosse, 2013). Due to the chaotic nature of the climatic system, each particle evolves in a different way. After the assimilation step, which is six months here, the likelihood of each member of the ensemble is evaluated according to its agreement with the climate inferred from the

CPD
9, 3953–3991, 2013

proxies. The assimilation frequency of six months has been chosen to follow more precisely the seasonal signal embedded in proxies as more than 60 % of the selected proxies represent a month or a particular season (mainly winter, summer, the hottest month or the coldest month). For each variable (i.e. air and sea surface temperature) the likelihood is estimated using anomalies obtained from both model and data as the difference between mid-Holocene (the period 5500–5000 y BP) and modern conditions (the period 950–450 y BP). This function is computed for all the locations and months for which paleodata is available. The particles that have the largest likelihood are retained. The other ensemble members are rejected. The remaining particles are resampled a number of times proportional to their likelihood in order to keep the number of particles constant and avoid a degenerative issue. For more details about the resampling method please refer to Dubinkina et al. (2011). A small perturbation of surface temperature is then added to the initial conditions of the members that have been sampled more than once, and the particles are propagated forward in time using the climate model. The whole procedure is repeated until the end of the simulated period (which corresponds to 400 yr here).

2.3 The proxy dataset

Numerous surface and sea surface temperature reconstructions derived from proxies are available for the Holocene. These reconstructions are derived from marine, continental and ice archives using different methods such as, among others, the Alkenone Paleothermometry (Grimalt and Lopez, 2007; Herbert, 2003), the modern Analog Technique (Brewer et al., 2007a) or the Stable Isotopes Analysis (Brook, 2007). Each quantitative reconstruction has its strengths and weaknesses (Birks et al., 2010; Juggins, 2013; Telford and Birks, 2005). For instance, almost all of them are influenced by the confounding effects, which means that environmental variables other than the climate variable of interest influence the reconstruction (Birks et al., 2010; Ortiz, 2007). For instance, a summer temperature derived from pollen records could include a signal related to winter temperature or precipitation (Birks et al., 2010). Furthermore, attributing

CPD
9, 3953–3991, 2013

the signal to a particular period of the year is not always straightforward as, for instance, the sedimentary alkenone signal is usually assumed to reflect the annually averaged sea surface temperature while at high latitudes the alkenone signal is likely phased to the summer months (Bendle and Rosell-Melé, 2007; Herbert, 2003; Samtleben and Bickert, 1990; Thomsen et al., 1998). In this study, we decided to follow the interpretation proposed in the original studies describing the proxies. For instance, if the reconstructed signal represents the summer surface air temperature according to the authors of those studies, this is also the case for us.

The proxy dataset used in the simulations with data assimilation results from a selection among more than 300 Holocene records according to the following criteria: (i) the record represents the air or the sea surface temperature, (ii) comes from archives located between 20° N and 90° N, (iii) has a mean temporal resolution of at least 250 yr for the mid-Holocene time-slice (6 ± 0.5 ky BP) and for the reference period (950 to 450 yr BP), as we work with anomalies related to this period (Sect. 2.2). (iv) If multiple reconstructions with different temporal interpretations are located within the same model grid, the seasonal reconstructions are retained, as we consider that it provides more information on the system. On the basis of these criteria, we have selected 50 records of air and sea surface temperature for the mid-Holocene (Table 1). For each selected record, an anomaly is calculated between the mean value of the period of interest (6 ± 0.5 ky BP) and the mean value of the reference period (500 yr) (Fig. 1). As we perform averages over periods that are longer than the dating uncertainties of the records, we neglect any potential biases related to those dating uncertainties.

Furthermore, if two reconstructions which represent the same physical variable at the same period of the year are located in the same model grid, they are merged. This is the case for the proxies number 2 (hereafter N2) and N2′ which are merged under the identifier N2. In the evaluation of the likelihood, we assume that the proxies represent the climate of the scale of the model grid, except for the reconstructions of Davis et al. (2003) and Viau and Gajewski (2009) which explicitly refer to a larger scale and, therefore, the average over the corresponding region for the model is performed

CPD
9, 3953–3991, 2013

before computing the model-data difference. Therefore, the signal reconstructed from the proxies is representative on a 3° grid box for CLIO3 and a 5.625° grid box for ECBilt2.

Finally, an estimation of the uncertainty for each reconstruction derived from proxies is required for data assimilation. This information is frequently not available, and when it is, these uncertainties are often very large and thus sometimes of the same order as the signal itself (Ohlwein and Wahl, 2011). As in Mathiot et al. (2013), we have thus deliberately selected here lower bounds for those uncertainties in order to provide a strong constraint on the model during the data assimilation process. By simplicity, we have also chosen only one error for each proxy type (Table 1) based on values provided in previous studies (e.g., Heikkilä and Seppä, 2003; Martrat et al., 2007; Mathiot et al., 2013; Müller et al., 1998; Seppä and Birks, 2001). Those values of the uncertainties affect weakly the spatial patterns but influence the magnitude of the changes induced by the data assimilation processes (Goosse et al., 2012). This will be taken into account in the interpretation of our results.

2.4 Experimental design

Three mid-Holocene simulations with data assimilation are performed and compared to a mid-Holocene reference simulation realized with LOVECLIM, named NODATA (Table 2). In two simulations either the continental or the oceanic proxies are assimilated and in one simulation these proxies are assimilated together. They are named CON, OCE and ALL, respectively. The objective is to propose two extreme cases in which we either constrain the model by only the continental archives or by only the signal inferred from oceanic proxies in order to identify the signal brought by each subset as well as the compatibility between model physics and the proxies, and between the proxies themselves. In addition, a simulation spanning the reference period (950 to 450 yr BP) is required as the likelihood in the data assimilation process compares proxy anomalies with modeled anomalies (Sect. 2.2). This simulation is driven by both natural and anthropogenic forcings as in Crespin et al. (2013).

CPD
9, 3953–3991, 2013

We also analyse simulations performed with GCMs to allow the comparison of the LOVECLIM results with the ones from three state-of-the-art models: BCC-CSM1-1, CSIRO-Mk3L-1-2 and MPI-ESM-P. For details about these models, please refer to the references listed in Table 2. These models were chosen because at the time of our analysis they were the only ones on the CMIP5 data portal that provide the variables needed for our diagnostics over the period 950–450 yr BP and the mid-Holocene.

The four mid-Holocene simulations performed with LOVECLIM are either 200 yr (NODATA) or 400 yr long (ALL, CON and OCE). The lenght of the simulation NODATA is smaller because it is the prolongation of an equilibrium simulation in the same conditions. The four simulations are driven by the same constant forcing which is identical to the one used by Mathiot et al. (2013). The orbital parameters follow Berger (1978). The greenhouse gas concentrations are based on the data of Flückiger et al. (2002). The Laurentide ice sheet topography and surface albedo have been adapted for LOVECLIM by Renssen et al. (2009) from the reconstruction of Peltier (2004). In comparison to the present, the changes in topography and surface albedo are extremely small. As in Mathiot et al. (2013) small fresh water fluxes (26 mSv) coming from the Antarctic ice sheet are added in the Amundsen, the Bellingshausen and the West part of Weddell Seas, based on Pollard and DeConto (2009). For the Northern Hemisphere, there are no fresh water fluxes resulting from the melt of the Laurentide ice sheet for this period (as in Renssen et al., 2009). This design is slightly different from the PMIP3 protocol used in GCMs as the latter assumed a similar ice sheet topography as the present one and no additional freshwater fluxes from ice sheet melting. But this has only a very marginal effect on our results at 6 ky BP.

CPD
9, 3953–3991, 2013

3 Results and discussion

3.1 Simulations without data assimilation

The climate anomalies simulated by LOVECLIM and the selected GCMs for mid-Holocene conditions display similar large-scale patterns (Fig. 2) and are consistent with previous modeling studies (e.g., Braconnot et al., 2007a). They all depict warmer air and sea surface temperature during the mid-Holocene summer and cooler air surface temperature during the winter, except in the Arctic. The mid-Holocene seasonal cycle amplitude is then more pronounced than the one of the reference period for most of the location in the Northern Hemisphere. This signal is mainly caused by the higher (lower) summer (winter) insolation for mid-Holocene (Braconnot et al., 2007a; Wanner et al., 2008). The winter Arctic warming is due to a memory effect associated with the summer insolation as the latter induces a decrease in ice thickness which leads to larger oceanic heat fluxes during the autumn and the winter, and then to a surface temperature increase during these seasons (Renssen et al., 2005).

In comparison with the first half of the last millennium, the westerlies are slightly weakened during the mid-Holocene in LOVECLIM in winter (Fig. 3). This appears consistent with smaller meridional gradient in temperature due to the Arctic warming and leads to a tendency towards more negative NAO state in the model for that period. BCC-CSM1-1 also shows a weakening of the westerlies in the Pacific during the mid-Holocene while MPI-ESM-P and CSIRO-Mk3L-1-2 show a slight strengthening. These results are consistent with an analysis of PMIP2 simulations realized by Gladstone et al. (2005) showing that many models display anomalies similar to either positive or negative NAO phases during the mid-Holocene compared to present day but without a clear and robust signal common between the different models.

The mid-Holocene reconstruction based on proxies (Fig. 2) depicts a less homogeneous pattern than the modeled one. The Arctic and Northern Europe surface air temperature are warmer during the summer and the winter which is in agreement with model results, while the Norwegian sea surface temperature is colder in the selected

CPD
9, 3953–3991, 2013

proxies for the same seasons, in contrast to model results. Risebrobakken et al. (2003) argue that this reconstructed cooling in the Norwegian sea may rather represent a subsurface signal, explaining the discrepancy with other estimates of surface temperature in the region. Over Europe, the northern part is warmer during the mid-Holocene and the southern one is colder all year long in the proxy-based reconstruction. Those changes are relatively consistent with the simulation results in winter, although the signal at high latitudes appears underestimated in many models, but no model is able to reproduce a cooling in summer over Southern Europe. In the western North Atlantic, reconstructed sea surface temperature is warmer, which is consistent in summer but not with the winter signal simulated by LOVECLIM and BCC-CSM1-1. In North America, surface temperature is slightly warmer in the reconstructions over the western part while it is colder over the eastern part, a signal that appears thus weaker than the one simulated by models.

A more quantitative model-data comparison shows that the magnitude of the signal (estimated here by the standard deviation of the anomalies) is much weaker in models, with a mean value of 0.9 °C, than in reconstructions based on proxies which reach a value of 1.6 °C (Fig. 4). The difference is seen both for continental and oceanic proxies but is more marked over the ocean where the signal in the proxies is 4.5 times greater than one of models, a result consistent with the recent findings of Lohmann et al. (2012). According to Fig. 4, the mean signal recorded by the selected proxies is larger over the ocean that over land by about 0.5 °C. This might appear surprising as the oceanic response to many forcings is expected to be smaller than the one over continents because of the larger thermal inertia of the ocean and of various feedbacks (e.g., Boer, 2011). Investigating in detail this issue is out of the scope of this study but it might be related to the too small number of proxies used here to estimate precisely the mean over oceans and continents or to the location of oceanic proxies that represent relatively local-regional phenomena in coastal areas or close to fronts and thus not the mean open ocean conditions.

CPD
9, 3953–3991, 2013

Additional information on the local agreement between model results and proxy reconstructions can be obtained by computing the Root Mean Square Error (RMSE) defined as

$$\mathrm{RMSE} = \sqrt{\frac{\sum_{i=1}^{n}\left(\Delta T_i^{\mathrm{mod}} - \Delta T_i^{\mathrm{obs}}\right)^2}{n}} \quad (1)$$

where n is the number of proxies, $\Delta T_i^{\mathrm{obs}}$ is one particular mid-Holocene air or sea surface temperature anomaly derived from a proxy record and $\Delta T_i^{\mathrm{mod}}$ is the corresponding modeled value. The minimum RMSE value for the different models is 1.7 °C (Fig. 4). This is larger than the mean signal, showing that the models have nearly no skill at the local scale as discussed in Hargreaves et al. (2013). Furthermore, the RMSE is larger for the oceanic proxies than for continental proxies in all the models. Actually, models results are in much better agreement between themselves than with the proxies as the root mean square difference between different models, at locations for which proxies are available, is close to 0.6 °C on average (i.e. about a third of the RMSE shown in Fig. 4).

Nevertheless, this quantitative evaluation of model performance based on results at the grid scale could be considered as a too strong test on several aspects. First, it does not take into account proxies uncertainties. Second, any small spatial shift in the model response compared to data would lead to large errors (e.g., Guiot et al., 1999). Third, model results and proxy records do not necessarily represent the climate at the same scale, leading to difference in the recorded signal, in particular on its magnitude. As a consequence, we have divided for Fig. 5a all the proxies into three categories: (i) LOVECLIM agrees with the proxies with error bars, (ii) LOVECLIM agrees only with the sign of the proxy record anomaly, (iii) it does not agree with the sign of the proxy record anomaly. This is displayed for the LOVECLIM model but the results are similar for the three GCMs (not shown). This leads to much more encouraging results than the conclusions derived from the analysis of the RMSE since LOVECLIM mid-Holocene

CPD
9, 3953–3991, 2013

simulation agrees with the sign of the anomaly of about two thirds of the proxies. This agreement displays no clear dependance on the season, on the location of the proxies or on the type of the proxies.

3.2 Simulations with data assimilation

Although the results of simulations constrained by data assimilation will be presented in a quantitative way, our interpretation will often be more qualitative for the two following reasons. First, as mentioned in the methodology section, the proxies uncertainty selected here has a potential influence on the amplitude of the difference between the simulations with and without data assimilation. Second, the disagreement between LOVECLIM without data assimilation and proxies is large. Although some improvement are obtained due to data assimilation, it is not expected to have a model state which displays values fully consistent with proxy records. This would for instance require additional perturbations within the ensemble of simulations, for example in model parameters, and thus to develop a specific experimental design. This is out of the scope of this paper, as we would like to focus, in this first study devoted to the mid-Holocene climate, on an estimate of the compatibilities between models and proxies.

By construction, the data assimilation method applied in LOVECLIM for the mid-Holocene period provides with results that are locally more consistent with the proxies that are assimilated than with any other simulation performed without data assimilation selected in this study (Fig. 4). Indeed, the simulation constrained by all the proxies, displays the RMSE of 1.6 °C which is 15 % closer to the proxy anomalies compared to the model without data assimilation. The RMSE between this simulation and the proxies is thus of the same magnitude as the mean signal of the proxies from the mid-Holocene (1.6 °C). The assimilation of the continental proxies alone gives the RMSE of 1.5 °C, which corresponds to a reconstruction which is 22 % closer to the proxies that are assimilated compared to the model without data assimilation. Finally, the data assimilation of the oceanic proxies alone provides with a reconstruction that is 15 %

CPD
9, 3953–3991, 2013

closer to those oceanic proxies, inducing almost a doubling of the simulated oceanic signal compared to the simulation without data assimilation.

The Fig. 4 shows also that the assimilation process in ALL leads LOVECLIM to be more consistent with the continental proxies than with the oceanic ones, which is due to the combination of two effects. First, the estimated error of the continental proxies is smaller than the oceanic records (Table 1), which means that in the computation of the likelihood a larger weight is given to the continental archives. Second, the model atmospheric fields and the surface temperature over land have a greater variance than the oceanic ones. Among the ensemble of simulations, it is thus more common to have members that are in agreement with continental proxies. This leads to a larger impact from the continental proxies if both domains are assimilated together and strong similarities between the simulation constrained by all the proxies and the one that is based on the continental proxies only.

Although data assimilation only marginally reduces the RMSE between model and data, the amount of proxies for which LOVECLIM does not agree with the sign of the anomalies decreases by about 20 % in OCE and about 30 % in CON and ALL compared to NODATA (Fig. 5). This is mainly caused in the reconstruction CON and ALL by a slight summer warming over North-East Europe, the Barents sea and the Kara sea and by a summer cooling around Lake Baikal as well as by a winter warming from North-East Europe to Lake Baikal, over North of Greenland and over the central part of North America (Fig. 6). In these simulations, the improvement of sea surface temperature is mainly related to a warming along the coast of North-America at about 40° N. In the simulation OCE the higher number of proxies that have the same anomalies as the model is mainly due to an annual warming of the North Atlantic and a summer warming in the North Pacific close to the West coast at 45° N (Fig. 6). Consequently, data assimilation drives the LOVECLIM model to a state which is maybe still not in the range of the anomalies derived from the proxies but that is at least more consistent with the sign of their changes.

CPD
9, 3953–3991, 2013

The three experiments with data assimilation also allow us testing the influence of the data assimilation over the different domains (continent and ocean) on all the proxy by grouping them in three categories (Fig. 7), but on different basis compared to the Fig. 5. The first category consists of proxies for which LOVECLIM results without data assimilation were already consistent with the proxies signal, i.e. the difference between model results and proxy-based reconstruction is smaller than the error assigned here. Moreover, assimilation of these proxies does not deteriorate the consistency between the model results with data assimilation and the signal recorded by the proxies. This category concerns 22 % of all the proxies used in this study. These proxy records can be identified individually on the basis of the numbers on the Fig. 1, using the Table 1. The second category (45 % of all the proxies) deals with the proxies that satisfy the two following criteria: (i) at least in one of the two simulations performed with data assimilation in which these proxies are used, they are more consistent with the results with data assimilation than with the results without data assimilation. (ii) These proxies are not less consistent with the results with data assimilation than with the results without data assimilation if they do not comply with the first rule. This corresponds to all the continental (oceanic) proxies for which the anomaly difference in absolute value decreases by at least 5 % in ALL and/or CON (ALL and/or OCE) and does not increase by more than 5 % in the other(s) simulation(s) with data assimilation. For 66 % of the proxies included in this category (28 % of all the proxies), the anomalies in the three simulations with data assimilation are closer to the proxy record anomaly than in the model without data assimilation. This implies that the model dynamics is able to propagate the signal brought by the assimilated proxies towards the locations where no data is assimilated and also that the information brought by these 28 % of proxies is coherent. The third category (33 % of all the proxies) includes the proxies that are either (i) less consistent (5 % threshold) with at least one of the three simulations with data assimilation compared with the simulation without data assimilation, or that are (ii) not more consistent with any simulation with data assimilation than with the simulation without data assimilation. In the majority of the cases (70 % of the proxies

CPD
9, 3953–3991, 2013

of this category), this corresponds to proxies on land (ocean) whose differences with model results are larger in OCE (CON) than in NODATA. As a consequence, the model dynamics suggests an incompatibility between the signal recorded by different types of proxies as improving one realm (land or ocean) deteriorates the results in the other one. This could be due to several processes such as a bias in the teleconnections simulated by the models, in the interpretation of the proxy signal, in the way models and proxies are compared. Our experimental design does not allow us determining which of those is dominant for each proxy record but it indicates that a special attention has to be given to those regions to understand the causes of this disagreement. This is the case, for instance, for the continental proxy N42 whose signal is opposite to the one depicted by the oceanic proxies N4, N7, N9 and N10. Another example is the oceanic proxy N15 whose signal shows a summer negative anomaly opposite to the positive one illustrated by the nearby continental proxies. This incompatibility consolidates the interpretation of Risebrobakken et al. (2003) that this proxy record should not be considered as an estimate of surface temperature. Finally, the proxies that are never more consistent with the simulations performed with data assimilation, indicate a profound disagreement between their information and the model physics. For instance, the model is not able to reproduce the summer (winter) cooling over the Southern-West (Northern-West) Europe depicted by the proxies N43 (N38) with data assimilation as already mentioned for LOVECLIM and the GCMs without data assimilation.

The improvement brought by data assimilation can be related to modifications of both winds and ocean currents. The atmospheric circulation changes associated with data assimilations in ALL, CON and OCE have a lower magnitude that the one in response to the forcing in NODATA for the summer, while for the winter, these changes are at least of the same magnitude as the model response to forcing (Fig. 8). All the experiments constrained by data assimilation display a decrease in geopotential height at high latitudes and an increase at mid latitudes in winter compared to NODATA, the signal in summer being weaker. This strengthens the westerlies over the North Atlantic inducing a winter warming from the Northern Europe to the Lake Baikal as well

CPD
9, 3953–3991, 2013

as over North America (Fig. 6). This is consistent with the findings of Rimbu et al. (2003), who indicate, using alkenone data, that the NAO was more likely in a positive pattern phase during the mid-Holocene with respect to our reference period. The induced surface temperature changes are more pronounced during the winter since during these months the atmospheric circulation endures the stronger changes. Furthermore, changes in atmospheric circulation are stronger in the OCE simulation than in the simulations ALL and CON (Fig. 8). This induces stronger westerlies over the Pacific and, therefore, a stronger warming over North America (Fig. 6). In winter the pattern over the North Atlantic is more complex in OCE than in the other experiments, with stronger westerlies northward of 50° N and weaker ones between 40° N and 50° N.

The spatial structure of the changes of annual mean sea surface temperature and surface current between each simulation performed with data assimilation and the simulation NODATA are similar, both in the North Atlantic and the North Pacific. Therefore, the figures are shown only for ALL (Fig. 9). In the Pacific, the strengthening of the westerlies produces an intensification of the northern branch of the North Pacific Gyre, which is stronger on the eastern part compared to the western part. This tends (i) to transport the warmer water from the northern extension of the Kuroshio eastward (around 45° N). It leads to warmer sea surface temperature and a warming of the atmosphere by the ocean. (ii) This also transports the colder western and northern Pacific water (cooled by the Siberian winds) toward the warmer eastern Pacific following the gyre cycle. The pattern is most marked in the simulation OCE than in the others two (Fig. 6) as the westerlies are more intensified in this simulation. Additionally, the northward shift of the westerlies slows down the winds around 30° N in the western Pacific which induces a reduced heat loss by evaporation and, therefore, a warmer sea surface temperature at this location. These two processes occur also in the Atlantic Ocean. The first is associated with an intensification of the gulf stream current at around 40° N due to stronger winds at this location (Fig. 8) which leads to a warming of the West Atlantic between 40° N and 50° N. The second one leads to a warming of the Atlantic between 20° N and 30° N induced by weaker winds. Finaly, around 65° N, a localized warming

CPD
9, 3953–3991, 2013

results from the ice front shifting. This feature is not robust as it is not present in all our experiments. The meridional overturning circulation is also slightly stronger in the Atlantic in the simulations with data assimilation compared to NODATA. The difference between the maximum in ALL-CON-OCE and the maximum in NODATA is, however, smaller than 1 Sv, which corresponds to an increase of the meridional heat transport at 30° S between 2 % (5 TW) and 8 % (18 TW) compared to the mean value in NODATA, contributing to some extent to the large-scale warming of the North Atlantic.

4 Conclusions

The conclusions derived from our analysis of simulations performed with GCMs and with LOVECLIM with and without data assimilation for the mid-Holocene can be summarized as follows:

1. In agreement with previous studies, a direct evaluation of the mean error of mid-Holocene simulations performed without data assimilation suggests that models have nearly no skill at the local scale compared to proxy data and that the models agree much better between themselves than with proxies. A comparison of the dominant patterns and of the sign of the changes, taking into account the uncertainties in proxies, leads to a much better consistency between models and data although clear disagreements remain in some regions.

2. The simulations with data assimilation are more consistent with the sign of the proxies anomalies and the spatial pattern of the changes than the simulation without data assimilation.

3. However, for a third of the proxies, data assimilation does not bring any improvement to the agreement with proxy data. For some proxies, it is due to a fundamental inconsistency with model physics, but for the majority of the proxies in this case, this is due to an incompatibility between the various proxies according

CPD
9, 3953–3991, 2013

to the model physics; i.e. the model is not able to follow the signal recorded in all of them simultaneously. One clear strength of our methodology is to identify objectively those proxies.

4. The methodology has also allowed identifying the mechanisms that lead to a better consistency between the model results and the proxies. The dominant one, which is robust in all our experiments, is the strengthening of the westerlies at mid-latitude that warms up the Northern Europe.

Acknowledgements. We thank all the people who made the data available, in particular Guillaume Leduc, Joan O. Grimalt, Belen Martrat and Heikki Seppä. We acknowledge the World Climate Research Programme's Working Group on Coupled Modelling, which is responsible for CMIP. For CMIP the US Department of Energy's Program for Climate Model Diagnosis and Intercomparison provides coordinating support and led development of software infrastructure in partnership with the Global Organization for Earth System Science Portals. We acknowledge D. Roche for making available the ice sheet forcing data for the LOVECLIM model. A. Mairesse also wishes to thank Marit-Solveig Seidenkrantz and Anne de Vernal for the very useful discussions about the oceanic proxies as well as Eric Wolff and Joël Guiot about the ice-cores and the pollen data, respectively. H. Goosse is Senior Research Associate with the Fonds National de la Recherche Scientifique (F.R.S. – FNRS-Belgium). The research leading to these results has received funding from the European Union's Seventh Framework programme (FP7/2007–2013) under grant agreement no. 243908, "Past4Future: Climate change – Learning from the past climate". Computational resources have been provided by the supercomputing facilities of the Université catholique de Louvain (CISM/UCL) and the Consortium des Equipements de Calcul Intensif en Fédération Wallonie Bruxelles (CECI) funded by FRS-FNRS. This is Past4Future contribution X.

References

Andreev, A. A., Tarasov, P. E., Siegert, C., Ebel, T., Klimanov, V. A., Melles, M., Bobrov, A. A., Dereviagin, A. Y., Lubinski, D. J., and Hubberten, H.-W.: Late Pleistocene and Holocene vegetation and climate on the northern Taymyr Peninsula, Arctic Russia, Boreas, 32, 484–505, 2003. 3955, 3980

CPD
9, 3953–3991, 2013

Antonsson, K., Brooks, S. J., Seppä, H., Telford, R. J., and Birks, H. J. B.: Quantitative palaeotemperature records inferred from fossil pollen and chironomid assemblages from Lake Gilltjärnen, northern central Sweden, J. Quaternary Sci., 21, 831–841, 2006. 3980

Barron, J. A., Heusser, L., Herbert, T., and Lyle, M.: High-resolution climatic evolution of coastal northern California during the past 16,000 years, Paleoceanography, 18, 1, doi:10.1029/2002PA000768, 2003. 3980

Bartlein, P. J., Harrison, S. P., Brewer, S., Connor, S., Davis, B. A. S., Gajewski, K., Guiot, J., Harrison-Prentice, T. I., Henderson, A., Peyron, O., Prentice, I. C., Scholze, M., Seppä, H., Shuman, B., Sugita, S., Thompson, R. S., Viau, A. E., Williams, J., and Wu, H.: Pollen-based continental climate reconstructions at 6 and 21 ka: a global synthesis, Clim. Dynam., 37, 775–802, 2011. 3954, 3955, 3956

Bendle, J. and Rosell-Melé, A.: High-resolution alkenone sea surface temperature variability on the North Icelandic Shelf: implications for Nordic Seas palaeoclimatic development during the Holocene, The Holocene, 17, 9–24, doi:10.1177/0959683607073269, 2007. 3959, 3980

Berger, A.: Long-term variations of daily insolation and quaternary climatic changes, J. Atmos. Sci., 35, 2362–2367, 1978. 3961

Birks, H., Heiri, O., Seppä, H., and Bjune, A.: Strengths and weaknesses of quantitative climate reconstructions based on late-Quaternary biological proxies, Open Ecology Journal, 3, 68–110, 2010. 3958

Boer, G.: The ratio of land to ocean temperature change under global warming, Clim. Dynam., 37, 2253–2270, 2011. 3963

Braconnot, P., Otto-Bliesner, B., Harrison, S., Joussaume, S., Peterchmitt, J.-Y., Abe-Ouchi, A., Crucifix, M., Driesschaert, E., Fichefet, Th., Hewitt, C. D., Kageyama, M., Kitoh, A., Laîné, A., Loutre, M.-F., Marti, O., Merkel, U., Ramstein, G., Valdes, P., Weber, S. L., Yu, Y., and Zhao, Y.: Results of PMIP2 coupled simulations of the Mid-Holocene and Last Glacial Maximum – Part 1: experiments and large-scale features, Clim. Past, 3, 261–277, doi:10.5194/cp-3-261-2007, 2007a. 3955, 3962

Braconnot, P., Otto-Bliesner, B., Harrison, S., Joussaume, S., Peterchmitt, J.-Y., Abe-Ouchi, A., Crucifix, M., Driesschaert, E., Fichefet, Th., Hewitt, C. D., Kageyama, M., Kitoh, A., Loutre, M.-F., Marti, O., Merkel, U., Ramstein, G., Valdes, P., Weber, L., Yu, Y., and Zhao, Y.: Results of PMIP2 coupled simulations of the Mid-Holocene and Last Glacial Maximum – Part 2: feedbacks with emphasis on the location of the ITCZ and mid- and high latitudes heat budget, Clim. Past, 3, 279–296, doi:10.5194/cp-3-279-2007, 2007b.

CPD
9, 3953–3991, 2013

Braconnot, P., Harrison, S., Kageyama, M., Bartlein, P., Masson-Delmotte, V., Abe-Ouchi, A., Otto-Bliesner, B., and Zhao, Y.: Evaluation of climate models using palaeoclimatic data, Nature Climate Change, 2, 417–424, 2012. 3955

Brewer, S., Guiot, J., and Barboni, D.: Pollen methods and studies: use of pollen as climate proxies, in: Encyclopedia of Quaternary Science, edited by: Elias, S. A., Elsevier, Oxford, 2497–2508, 2007a. 3958

Brewer, S., Guiot, J., and Torre, F.: Mid-Holocene climate change in Europe: a data-model comparison, Clim. Past, 3, 499–512, doi:10.5194/cp-3-499-2007, 2007b. 3955

Brook, E. J.: Ice core methods: overview, in: Encyclopedia of Quaternary Science, edited by: Elias, S. A., Elsevier, Oxford, 2497–2508, 2007. 3958

Brovkin, V., Ganopolski, A., and Svirezhev, Y.: A continuous climate-vegetation classification for use in climate-biosphere studies, Ecol. Model., 101, 251–261, 1997. 3957

Claussen, M., Kubatzki, C., Brovkin, V., Ganopolski, A., Hoelzmann, P., and Pachur, H.: Simulation of an abrupt change in Saharan vegetation in the mid-Holocene, Geophys. Res. Lett., 26, 2037–2040, 1999. 3955

Clegg, B. F., Clarke, G. H., Chipman, M. L., Chou, M., Walker, I. R., Tinner, W., and Hu, F. S.: Six millennia of summer temperature variation based on midge analysis of lake sediments from Alaska, Quaternary Sci. Rev., 29, 3308–3316, 2010. 3955

Crespin, E., Goosse, H., Fichefet, T., Mairesse, A., and Sallaz-Damaz, Y.: Arctic climate over the past millennium: annual and seasonal responses to external forcings, The Holocene, 23, 321–329, 2013. 3960, 3982

Crucifix, M.: Modelling the climate of the Holocene, in: Natural Climate variability and Global Warming: a Holocene Perspective, edited by: Battarbee, R. W. and Binney, H., Wiley-Blackwell, 98–122, Oxford, United Kingdom, 2008. 3955

Davis, B. A. S., Brewer, S., Stevenson, A. C., and Guiot, J.: The temperature of Europe during the Holocene reconstructed from pollen data, Quaternary Sci. Rev., 22, 1701–1716, 2003. 3954, 3955, 3959, 3981

deMenocal, P., Ortiz, J., Guilderson, T., and Sarnthein, M.: Coherent high- and low-latitude climate variability during the Holocene warm period, Science, 288, 2198–2202, 2000. 3980

Dubinkina, S. and Goosse, H.: An assessment of particle filtering methods and nudging for climate state reconstructions, Clim. Past, 9, 1141–1152, doi:10.5194/cp-9-1141-2013, 2013. 3957

CPD
9, 3953–3991, 2013

Dubinkina, S., Goosse, H., Sallaz-Damaz, Y., Crespin, E., and Crucifix, M.: Testing a particle filter to reconstruct climate changes over past centuries, Int. J. Bifurcat. Chaos, 21, 3611–3618, doi:10.1142/S0218127411030763, 2011. 3956, 3957, 3958

Esparza, M.: Estudi de la variabilitat climàtica de l'oceà Atlàntic nord durant l'holocè mitjançant biomarcadors moleculars, Master's thesis, Autonomous University of Barcelona, Faculty of Sciences, Bellaterra (Cerdanyola del Vallès), Barcelona, Spain, 2005. 3980

Flückiger, J., Monnin, E., Stauffer, B., Schwander, J., Stocker, T. F., Chappellaz, J., Raynaud, D., and Barnola, J.-M.: High-resolution Holocene N_2O ice core record and its relationship with CH_4 and CO_2, Global Biogeochem. Cy., 16, 10-1–10-8, 2002. 3961

Gladstone, R., Ross, I., Valdes, P., Abe-Ouchi, A., Braconnot, P., Brewer, S., Kageyama, M., Kitoh, A., Legrande, A., Marti, O., Otto-Bliesner, B., Peltier, W. R., and Vettoretti, G.: Mid-Holocene NAO: a PMIP2 model intercomparison, Geophys. Res. Lett., 32, L16707, doi:10.1029/2005GL023596, 2005. 3962

Goosse, H. and Fichefet, T.: Importance of ice-ocean interactions for the global ocean circulation: a model study, J. Geophys. Res., 104, 23337–23355, 1999. 3957

Goosse, H., Brovkin, V., Fichefet, T., Haarsma, R., Huybrechts, P., Jongma, J., Mouchet, A., Selten, F., Barriat, P.-Y., Campin, J.-M., Deleersnijder, E., Driesschaert, E., Goelzer, H., Janssens, I., Loutre, M.-F., Morales Maqueda, M. A., Opsteegh, T., Mathieu, P.-P., Munhoven, G., Pettersson, E. J., Renssen, H., Roche, D. M., Schaeffer, M., Tartinville, B., Timmermann, A., and Weber, S. L.: Description of the Earth system model of intermediate complexity LOVECLIM version 1.2, Geosci. Model Dev., 3, 603–633, doi:10.5194/gmd-3-603-2010, 2010. 3956, 3957, 3982

Goosse, H., Crespin, E., Dubinkina, S., Loutre, M.-F., Mann, M. E., Renssen, H., Sallaz-Damaz, Y., and Shindell, D.: The role of forcing and internal dynamics in explaining the "Medieval Climate Anomaly", Clim. Dynam., 39, 2847–2866, 2012. 3957, 3960

Grimalt, J. and Lopez, J.: Paleoceanography, biological proxies: alkenone paleothermometry from coccoliths, in: Encyclopedia of Quaternary Science, edited by: Elias, S. A., Elsevier, Oxford, 1610–1618, 2007. 3958

Guiot, J., Boreux, J.-J., Braconnot, P., and Torre, F.: Data-model comparison using fuzzy logic in paleoclimatology, Clim. Dynam., 15, 569–581, 1999. 3964

Harada, N., Ahagon, N., Sakamoto, T., Uchida, M., Ikehara, M., and Shibata, Y.: Rapid fluctuation of alkenone temperature in the southwestern Okhotsk Sea during the past 120 ky, Global Planet. Change, 53, 29–46, 2006. 3981

CPD
9, 3953–3991, 2013

Hargreaves, J. C., Annan, J. D., Ohgaito, R., Paul, A., and Abe-Ouchi, A.: Skill and reliability of climate model ensembles at the Last Glacial Maximum and mid-Holocene, Clim. Past, 9, 811–823, doi:10.5194/cp-9-811-2013, 2013. 3955, 3964

Heikkilä, M. and Seppä, H.: A 11,000 yr palaeotemperature reconstruction from the southern boreal zone in Finland, Quaternary Sci. Rev., 22, 541–554, 2003. 3960, 3980

Herbert, T.: Alkenone paleotemperature determinations, in: Treatise on Geochemistry, edited by: Holland, H. D. and Turekian, K. K., Pergamon, Oxford, 391–432, 2003. 3958, 3959

Isono, D., Yamamoto, M., Irino, T., Oba, T., Murayama, M., Nakamura, T., and Kawahata, H.: The 1500-year climate oscillation in the midlatitude North Pacific during the Holocene, Geology, 37, 591, doi:10.1130/G25667A.1, 2009. 3980

Jian, Z., Wang, P., Saito, Y., Wang, J., Pflaumann, U., Oba, T., and Cheng, X.: Holocene variability of the Kuroshio Current in the Okinawa Trough, northwestern Pacific Ocean, Earth Planet. Sc. Lett., 184, 305–319, 2000. 3980

Juggins, S.: Quantitative reconstructions in palaeolimnology: new paradigm or sick science?, Quaternary Sci. Rev., 64, 20–32, 2013. 3958

Kim, J., Meggers, H., Rimbu, N., Lohmann, G., Freudenthal, T., Müller, P., and Schneider, R.: Impacts of the North Atlantic gyre circulation on Holocene climate off northwest Africa, Geology, 35, 387, doi:10.1130/G23251A.1, 2007. 3980

Lauritzen, S. and Lundberg, J.: Calibration of the speleothem delta function: an absolute temperature record for the Holocene in northern Norway, The Holocene, 9, 659, doi:10.1191/095968399667823929, 1999. 3980

Leduc, G., Schneider, R., Kim, J.-H., and Lohmann, G.: Holocene and Eemian sea surface temperature trends as revealed by alkenone and Mg/Ca paleothermometry, Quaternary Sci. Rev., 29, 989–1004, 2010. 3954, 3956

Lohmann, G., Pfeiffer, M., Laepple, T., Leduc, G., and Kim, J.-H.: A model-data comparison of the Holocene global sea surface temperature evolution, Clim. Past Discuss., 8, 1005–1056, doi:10.5194/cpd-8-1005-2012, 2012. 3955, 3963

Marcott, S. A., Shakun, J. D., Clark, P. U., and Mix, A. C.: A Reconstruction of Regional and Global Temperature for the Past 11,300 Years, Science, 339, 1198–1201, 2013. 3954, 3955

Marsland, S., Haak, H., Jungclaus, J., Latif, M., and Röske, F.: The Max-Planck-Institute global ocean/sea ice model with orthogonal curvilinear coordinates, Ocean Model., 5, 91–127, 2003. 3982

CPD
9, 3953–3991, 2013

Martrat, B.: Studies of sedimentary organic matter to infer rapid climatic changes at the Barents and Iberian continental margins on centennial time resolution over the past four climate cycles of the Quaternary (ca. 420,000 years), Ph. D. thesis, UPC, CSIC, Barcelona, Spain, 2007. 3980

Martrat, B., Grimalt, J., Shackleton, N., de Abreu, L., Hutterli, M., and Stocker, T.: Four climate cycles of recurring deep and surface water destabilizations on the Iberian margin, Science, 317, 502–507, doi:10.1126/science.1139994, 2007. 3960, 3980

Mathiot, P., Goosse, H., Crosta, X., Stenni, B., Braida, M., Renssen, H., Van Meerbeeck, C. J., Masson-Delmotte, V., Mairesse, A., and Dubinkina, S.: Using data assimilation to investigate the causes of Southern Hemisphere high latitude cooling from 10 to 8 ka BP, Clim. Past, 9, 887–901, doi:10.5194/cp-9-887-2013, 2013. 3957, 3960, 3961

Mock, C. J.: Paleoclimate: introduction, why study paleoclimatology ?, in: Encyclopedia of Quaternary Science, edited: by Elias, S. A., Elsevier, 1867–1872, Oxford, United Kingdom, 2007. 3955

Müller, P. J., Kirst, G., Ruhland, G., von Storch, I., and Rosell-Melé, A.: Calibration of the alkenone paleotemperature index U37K based on core-tops from the eastern South Atlantic and the global ocean (60° N–60° S), Geochim. Cosmochim. Ac., 62, 1757–1772, 1998. 3960

Ohlwein, C. and Wahl, E.: Review of probabilistic pollen-climate transfer methods, Quaternary Sci. Rev., 31, 17–29, doi:10.1016/j.quascirev.2011.11.002, 2011. 3960

Opsteegh, J. D., Haarsma, R. J., Selten, F. M., and Kattenberg, A.: ECBILT: a dynamic alternative to mixed boundary conditions in ocean models, Tellus A, 50, 348–367, 1998. 3957

Ortiz, J. D.: Paleoceanography, biological proxies: temperature proxies, census counts, in: Encyclopedia of Quaternary Science, edited by: Elias, S. A., Elsevier, Oxford, 1692–1699, 2007. 3958

Pelejero, C., Grimalt, J., Heilig, S., Kienast, M., and Wang, L.: High-resolution UK37 temperature reconstructions in the South China Sea over the past 220 kyr, Paleoceanography, 14, 224–231, 1999. 3980

Peltier, W.: Global glacial isostasy and the surface of the ice-age Earth: the ICE-5G (VM2) model and GRACE, Annu. Rev. Earth Pl. Sc., 32, 111–149, 2004. 3961

Peros, M. and Gajewski, K.: Holocene climate and vegetation change on Victoria Island, western Canadian Arctic, Quaternary Sci. Rev., 27, 235–249, 2008. 3981

CPD
9, 3953–3991, 2013

Phipps, S. J., Rotstayn, L. D., Gordon, H. B., Roberts, J. L., Hirst, A. C., and Budd, W. F.: The CSIRO Mk3L climate system model version 1.0 – Part 1: Description and evaluation, Geosci. Model Dev., 4, 483–509, doi:10.5194/gmd-4-483-2011, 2011. 3982

Pollard, D. and DeConto, R.: Modelling West Antarctic ice sheet growth and collapse through the past five million years, Nature, 458, 329–332, 2009. 3961

Raddatz, T., Reick, C., Knorr, W., Kattge, J., Roeckner, E., Schnur, R., Schnitzler, K.-G., Wetzel, P., and Jungclaus, J.: Will the tropical land biosphere dominate the climate-carbon cycle feedback during the twenty-first century ?, Clim. Dynam., 29, 565–574, 2007. 3982

Renssen, H., Goosse, H., Fichefet, T., Brovkin, V., Driesschaert, E., and Wolk, F.: Simulating the Holocene climate evolution at northern high latitudes using a coupled atmosphere-sea ice-ocean-vegetation model, Clim. Dynam., 24, 23–43, 2005. 3962

Renssen, H., Seppä, H., Heiri, O., Roche, D., Goosse, H., and Fichefet, T.: The spatial and temporal complexity of the Holocene thermal maximum, Nat. Geosci., 2, 411–414, 2009. 3961

Renssen, H., Seppä, H., Crosta, X., Goosse, H., and Roche, D.: Global characterization of the Holocene Thermal Maximum, Quaternary Sci. Rev., 48, 7–19, 2012. 3955

Rimbu, N., Lohmann, G., Kim, J.-H., Arz, H. W., and Schneider, R.: Arctic/North Atlantic Oscillation signature in Holocene sea surface temperature trends as obtained from alkenone data, Geophys. Res. Lett., 30, 1280, doi:10.1029/2002GL016570, 2003. 3969

Risebrobakken, B., Jansen, E., Andersson, C., Mjelde, E., and Hevrøy, K.: A high-resolution study of Holocene paleoclimatic and paleoceanographic changes in the Nordic Seas, Paleoceanography, 18, 1017, doi:10.1029/2002PA000764, 2003. 3963, 3968, 3980

Rodrigues, T., Grimalt, J., Abrantes, F., Flores, J., and Lebreiro, S.: Holocene interdependences of changes in sea surface temperature, productivity, and fluvial inputs in the Iberian continental shelf (Tagus mud patch), Geochemistry, Geophysics, Geosystems, 10, doi:10.1029/2008GC002367, 2009. 3980

Sachs, J. P.: Cooling of Northwest Atlantic slope waters during the Holocene, Geophys. Res. Lett., 34, L03609, doi:10.1029/2006GL028495, 2007. 3980

Samtleben, C. and Bickert, T.: Coccoliths in sediment traps from the Norwegian Sea, Mar. Micropaleontol., 16, 39–64, 1990. 3959

Sarmaja-Korjonen, K. and Seppä, H.: Abrupt and consistent responses of aquatic and terrestrial ecosystems to the 8200 cal. yr cold event: a lacustrine record from Lake Arapisto, Finland, The Holocene, 17, 457–467, 2007. 3980

CPD
9, 3953–3991, 2013

Seppä, H. and Birks, H.: July mean temperature and annual precipitation trends during the Holocene in the Fennoscandian tree-line area: pollen-based climate reconstructions, The Holocene, 11, 527–539, 2001. 3955, 3960, 3980

Seppä, H. and Birks, H.: Holocene climate reconstructions from the Fennoscandian tree-line area based on pollen data from Toskaijavri, Quaternary Res., 57, 191–199, 2002. 3955, 3980

Seppä, H. and Poska, A.: Holocene annual mean temperature changes in Estonia and their relationship to solar insolation and atmospheric circulation patterns, Quaternary Res., 61, 22–31, 2004. 3980

Seppä, H., Hammarlund, D., and Antonsson, K.: Low-frequency and high-frequency changes in temperature and effective humidity during the Holocene in south-central Sweden: implications for atmospheric and oceanic forcings of climate, Clim. Dynam., 25, 285–297, 2005. 3980

Tarasov, P. E., Bezrukova, E. V., and Krivonogov, S. K.: Late Glacial and Holocene changes in vegetation cover and climate in southern Siberia derived from a 15 kyr long pollen record from Lake Kotokel, Clim. Past, 5, 285–295, doi:10.5194/cp-5-285-2009, 2009. 3981

Telford, R. and Birks, H.: The secret assumption of transfer functions: problems with spatial autocorrelation in evaluating model performance, Quaternary Sci. Rev., 24, 2173–2179, 2005. 3958

Thomsen, C., Schulz-Bull, D., Petrick, G., and Duinker, J.: Seasonal variability of the long-chain alkenone flux and the effect on the Uk37-index in the Norwegian Sea, Organic Geochemistry, 28, 311–323, 1998. 3959

Thornalley, D., Elderfield, H., and McCave, I.: Holocene oscillations in temperature and salinity of the surface subpolar North Atlantic, Nature, 457, 711–714, 2009. 3980

Viau, A. E. and Gajewski, K.: Reconstructing millennial-scale, regional paleoclimates of Boreal Canada during the Holocene., J. Climate, 22, 316–330, 2009. 3954, 3959, 3981

Vinther, B., Buchardt, S., Clausen, H., Dahl-Jensen, D., Johnsen, S., Fisher, D., Koerner, R., Raynaud, D., Lipenkov, V., and Andersen, K.: Holocene thinning of the Greenland ice sheet, Nature, 461, 385–388, 2009. 3954, 3955, 3981

Wanner, H., Beer, J., Bütikofer, J., Crowley, T., Cubasch, U., Flückiger, J., Goosse, H., Grosjean, M., Joos, F., Kaplan, J., Küttel, M., Müller, S., Prentice, I., Solomina, O., Stocker, T., Tarasov, P., Wagner, M., and Widmann, M.: Mid-to Late Holocene climate change: an overview, Quaternary Sci. Rev., 27, 1791–1828, 2008. 3962

CPD
9, 3953–3991, 2013

Zhao, Y., Braconnot, P., Marti, O., Harrison, S., Hewitt, C., Kitoh, A., Liu, Z., Mikolajewicz, U., Otto-Bliesner, B., and Weber, S.: A multi-model analysis of the role of the ocean on the African and Indian monsoon during the mid-Holocene, Clim. Dynam., 25, 777–800, 2005. 3955

CPD
9, 3953–3991, 2013

Table 1. Air surface (TS) and sea surface (SST) mid-Holocene temperature proxies used in the simulations with data assimilation. Winter corresponds to December to February (DJF) and summer to June to August (JJA). The anomalies and their error are in °C.

id	lat	lon	Site or core name	Area	Proxy record	Climate variable	Temporal interpretation	6 ky BP ano.	error	Reference
1	61.48	26.07	Laihalampi lake	Southern Finland	Pollen	TS	Annual	1.86	0.60	(Heikkilä and Seppä, 2003)
2	69.20	21.47	Toskaljavri lake	Northern Finland	Pollen	TS	Jul	1.06	0.60	(Seppä and Birks, 2002)
2'	68.68	22.08	Tsuolbmajavri lake	Northern Finland	Pollen	TS	Jul	1.14	0.60	(Seppä and Birks, 2001)
3	55.65	−13.98	Feni Drift	North Atlantic	Alkenone – Uk37	SST	Annual	0.47	0.80	(Esparza, 2005)
4	40.50	4.03	Minorca	Mediterranean	Alkenone – Uk37	SST	Annual	2.38	0.80	(Martrat, 2007)
5	43.88	−62.80	OCE326-GGC30	Northwest Atlantic	Alkenone – Uk37	SST	Annual	4.15	0.80	(Sachs, 2007)
6	43.48	−54.87	OCE326-GGC26	Northwest Atlantic	Alkenone – Uk37	SST	Annual	2.81	0.80	(Sachs, 2007)
7	37.56	−10.14	MD01-2444	Iberian Margin	Alkenone – Uk37	SST	Annual	0.63	0.80	(Martrat et al., 2007)
8	66.60	−17.58	JR51-GC35	Nordic Seas	Alkenone – Uk37	SST	Annual	−1.10	0.80	(Bendle and Rosell-Melé, 2007)
9	30.85	−10.27	GeoB 6007-02	Northwest Africa	Alkenone – Uk37	SST	Annual	1.02	0.80	(Kim et al., 2007)
10	38.63	−9.45	D13882	Iberian Margin	Alkenone – Uk37	SST	Annual	2.27	0.80	(Rodrigues et al., 2009)
11	62.09	−17.82	RAPiD-12-1k	Subpolar North Atlantic	Mg/Ca and d18O (bulloides)	SST	May, Jun	−1.12	0.80	(Thornalley et al., 2009)
12	60.08	15.83	Stora Gilltjarnen	Sweden	Pollen	TS	Annual	1.01	0.60	(Antonsson et al., 2006)
13	60.58	24.08	Lake Arapisto	Finland	Pollen	TS	Annual	3.04	0.60	(Sarmaja-Korjonen and Seppä, 2007)
14	58.55	13.67	Lake Flarken	Sweden	Pollen	TS	Annual	2.04	0.60	(Seppä et al., 2005)
15	66.97	7.63	JM97-948/2A and MD95-2011	Norwegian Sea	Forams (planktic)	SST	August	−1.77	0.80	(Risebrobakken et al., 2003)
16	74.47	98.63	Levinson-Lessing lake	Russia	Pollen	TS	Annual	2.06	0.60	(Andreev et al., 2003)
17	41.68	−124.93	ODP1019C	North Pacific	Alkenone – Uk37	SST	Annual	−0.84	0.80	(Barron et al., 2003)
18	20.75	−18.58	ODP658C	Northwest Africa Sea	Forams (planktic)	SST	Aug	−3.05	0.80	(deMenocal et al., 2000)
19	20.75	−18.58	ODP658C	Northwest Africa Sea	Forams (planktic)	SST	Feb	−1.07	0.80	(deMenocal et al., 2000)
20	31.48	128.52	Core B-3GC	Northwestern Pacific Ocean	Forams (planktic)	SST	Summer	−0.54	0.80	(Jian et al., 2000)
21	31.48	128.52	Core B-3GC	Northwestern Pacific Ocean	Forams (planktic)	SST	Winter	−1.59	0.80	(Jian et al., 2000)
22	66.55	13.92	SG93	Norway (Soylegrotta)	Speleothem	TS	Annual	−0.19	0.80	(Lauritzen and Lundberg, 1999)
23	58.58	26.65	Raigastvere lake	Estonia	Pollen	TS	Annual	2.63	0.60	(Seppä and Poska, 2004)
24	36.03	141.78	KR02-06 St.A MC/GC and MD01-2421	Northwestern Pacific	Alkenone – Uk37	SST	Summer	2.08	0.80	(Isono et al., 2009)
25	20.12	117.38	GIK17940-2	South China Sea	Alkenone – Uk37	SST	Annual	−0.19	0.80	(Pelejero et al., 1999)

CPD
9, 3953–3991, 2013

Table 1. Continued.

id	lat	lon	Site or core name	Area	Proxy record	Climate variable	Temporal interpretation	6 ky BP ano.	error	Reference
26	52.78	108.12	Kotokel lake	Russia	Pollen	TS	Jan	3.30	0.60	(Tarasov et al., 2009)
27	52.78	108.12	Kotokel lake	Russia	Pollen	TS	Jul	−0.07	0.60	(Tarasov et al., 2009)
28	80.70	−73.70	Agassiz Ice cap	Greenland	ice core – d18O	TS	Annual	2.00	0.40	(Vinther et al., 2009)
29	71.27	−26.73	Renland Ice Cap	Greenland	ice core – d18O	TS	Annual	2.00	0.40	(Vinther et al., 2009)
30	50 to 70	−65 to −50	Labrador region	Canada	Pollen	TS	Jan	−2.28	0.60	(Viau and Gajewski, 2009)
31	50 to 70	−65 to −50	Labrador region	Canada	Pollen	TS	Jul	−0.48	0.60	(Viau and Gajewski, 2009)
32	50 to 70	−120 to −80	Central Canada region	Canada	Pollen	TS	Jan	0.68	0.60	(Viau and Gajewski, 2009)
33	50 to 70	−120 to −80	Central Canada region	Canada	Pollen	TS	Jul	0.49	0.60	(Viau and Gajewski, 2009)
34	50 to 70	−140 to −120	MacKenzie region	Canada	Pollen	TS	Jan	0.46	0.60	(Viau and Gajewski, 2009)
35	50 to 70	−140 to −120	MacKenzie region	Canada	Pollen	TS	Jul	0.17	0.60	(Viau and Gajewski, 2009)
36	44.53	145.00	MD01-2412	Okhotsk Sea	Alkenone – Uk37	SST	Autumn	−0.82	0.80	(Harada et al., 2006)
37	71.34	−113.78	KR02 lake	Victoria Island (Canada)	Pollen	TS	Jul	0.00	0.60	(Peros and Gajewski, 2008)
38	55 to 72	−12 to 15	Northwest region	Europe	Pollen	TS	Winter	−0.71	0.60	(Davis et al., 2003)
39	55 to 72	−12 to 15	Northwest region	Europe	Pollen	TS	Summer	1.00	0.60	(Davis et al., 2003)
40	45 to 55	−12 to 15	Centralwest region	Europe	Pollen	TS	Winter	−0.51	0.60	(Davis et al., 2003)
41	45 to 55	−12 to 15	Centralwest region	Europe	Pollen	TS	Summer	0.47	0.60	(Davis et al., 2003)
42	30 to 45	−12 to 15	Southwest region	Europe	Pollen	TS	Winter	−0.98	0.60	(Davis et al., 2003)
43	30 to 45	−12 to 15	Southwest region	Europe	Pollen	TS	Summer	−1.49	0.60	(Davis et al., 2003)
44	55 to 72	15 to 50	Northeast region	Europe	Pollen	TS	Winter	0.22	0.60	(Davis et al., 2003)
45	55 to 72	15 to 50	Northeast region	Europe	Pollen	TS	Summer	0.60	0.60	(Davis et al., 2003)
46	45 to 55	15 to 50	Centraleast region	Europe	Pollen	TS	Winter	0.24	0.60	(Davis et al., 2003)
47	45 to 55	15 to 50	Centraleast region	Europe	Pollen	TS	Summer	−0.11	0.60	(Davis et al., 2003)
48	30 to 45	15 to 50	Southeast region	Europe	Pollen	TS	Winter	−0.25	0.60	(Davis et al., 2003)
49	30 to 45	15 to 50	Southeast region	Europe	Pollen	TS	Summer	−0.66	0.60	(Davis et al., 2003)

CPD
9, 3953–3991, 2013

Table 2. List of the simulations analysed in this study.

Model name	simulation period	simulation name	Forcing	Data assimilation	Reference
LOVECLIM	reference	LMALL	Crespin et al. (2013)	no	Goosse et al. (2010)
	mid-Holocene	ALL	this study	yes	
	mid-Holocene	CON	this study	yes	
	mid-Holocene	OCE	this study	yes	
	mid-Holocene	NODATA	this study	no	
MPI-ESM-P	reference	past1000	PMIP3	no	Raddatz et al. (2007); Marsland et al. (2003)
	mid-Holocene	midHolocene	PMIP3	no	
CSIRO-Mk3L-1-2	reference	past1000	PMIP3	no	Phipps et al. (2011)
	mid-Holocene	midHolocene	PMIP3	no	
BCC-CSM1-1	reference	past1000	PMIP3	no	http://bcc.cma.gov.cn/bcccsm/web/?ChannelID=43
	mid-Holocene	midHolocene	PMIP3	no	

CPD
9, 3953–3991, 2013

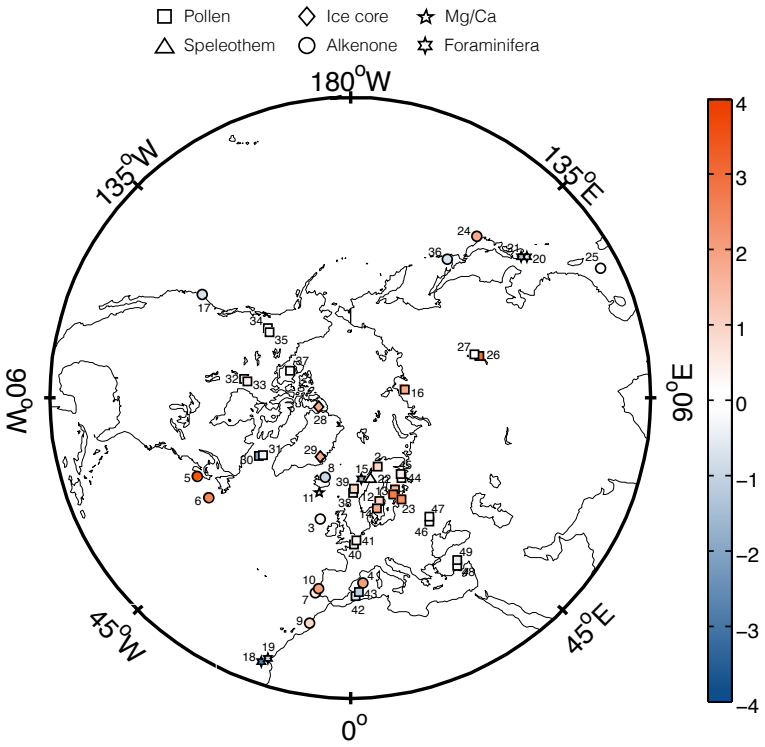

Fig. 1. Mean air and sea surface temperature anomaly (°C) for all the proxies available for the mid-Holocene. Each marker type corresponds to a different proxy group. Each anomaly represents a month or a particular period (Table 1). If more than one proxy record is given at the same location, the markers representing the proxies are slightly shifted for improved readability. The reference period is 950 to 450 yr BP.

CPD
9, 3953–3991, 2013

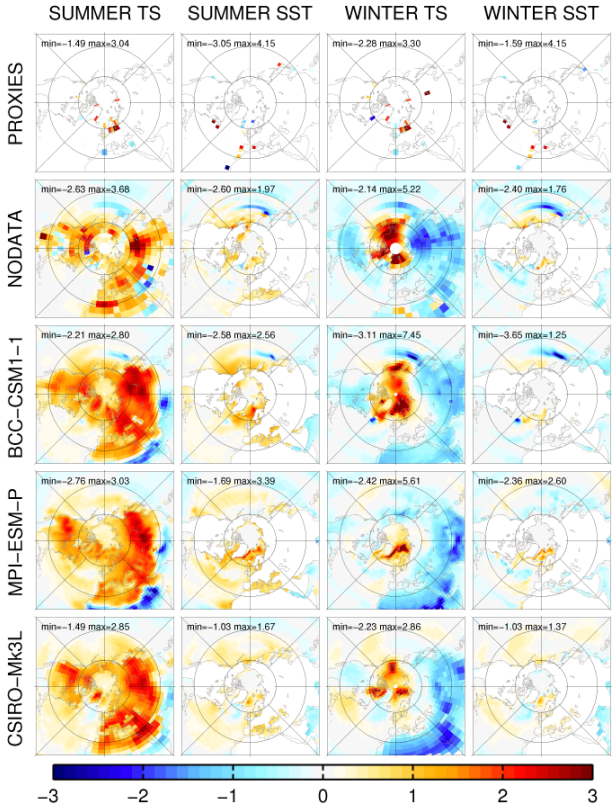

Fig. 2. Mid-Holocene air (TS) and sea (SST) surface temperature anomaly (°C) for the proxies, LOVECLIM without data assimilation (NODATA) and the GCMs. Winter corresponds to December to February (DJF) and summer to June to August (JJA). The reference period is 950 to 450 yr BP.

CPD
9, 3953–3991, 2013

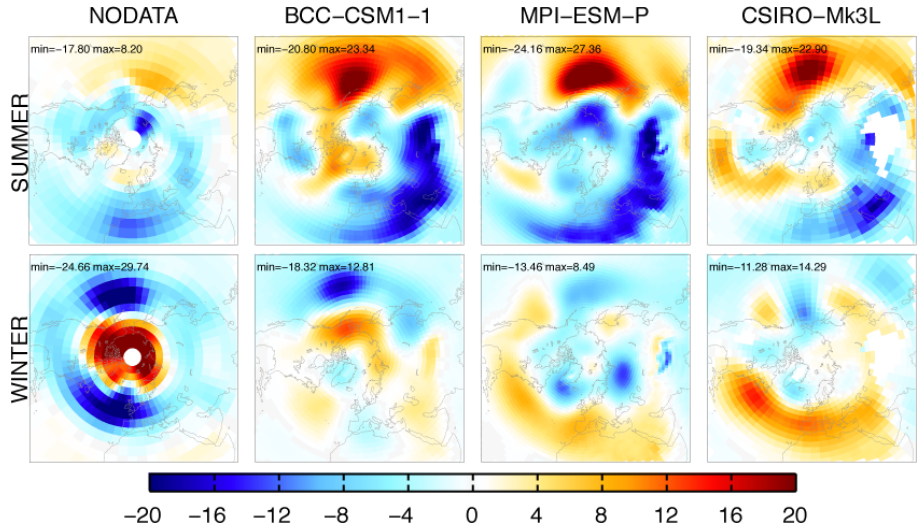

Fig. 3. Mid-Holocene geopotential height anomaly (in m) at 800 hPa for LOVECLIM without data assimilation (NODATA) and at 850 hPa for the GCMs. Winter corresponds to December to February (DJF) and summer to June to August (JJA). The reference period is 950 to 450 yr BP.

CPD
9, 3953–3991, 2013

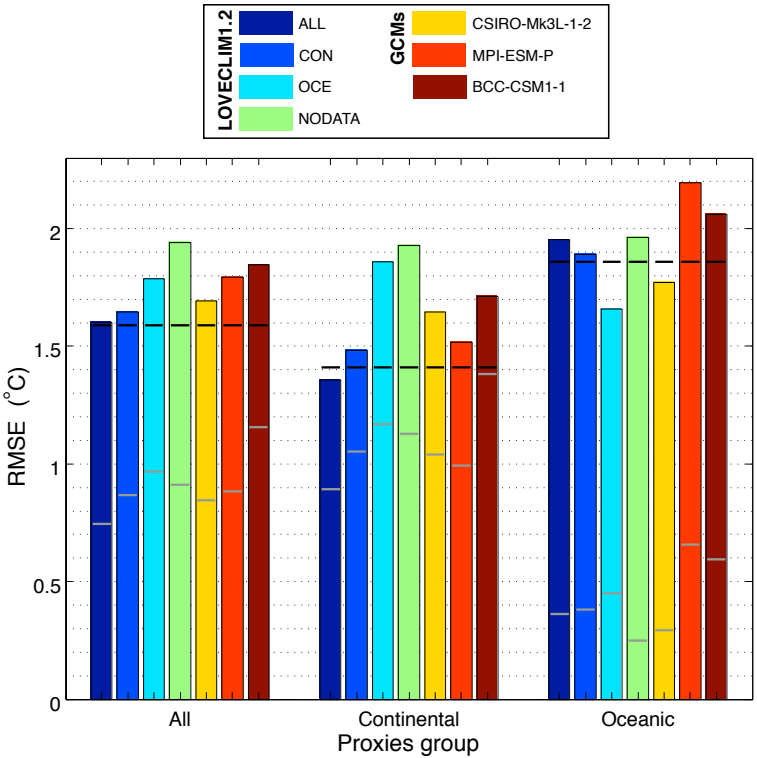

Fig. 4. From left to right: RMSE between the mid-Holocene anomalies of each simulation (LOVECLIM with and without data assimilation and the GCMs) and the proxies anomalies for three groups of proxies: all the proxies, the continental proxies only and the oceanic proxies only. The mean mid-Holocene signal (estimated as the standard deviation of the anomalies) for the proxies and the model are the black and the grey horizontal bars, respectively.

CPD
9, 3953–3991, 2013

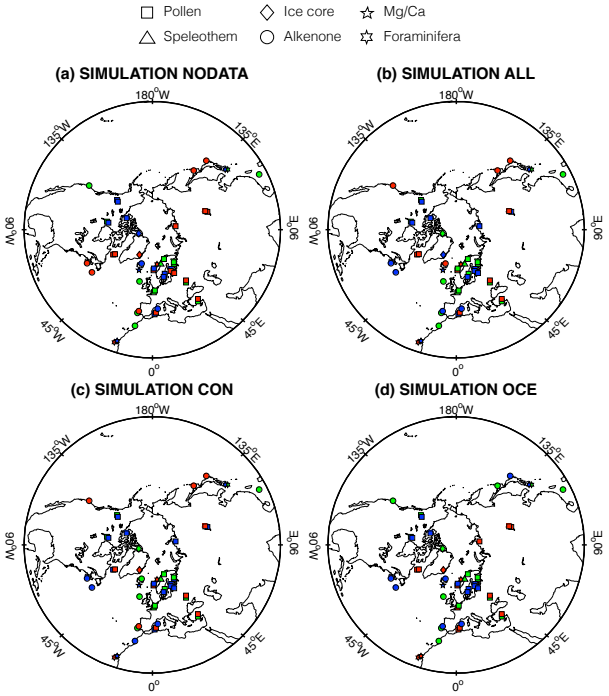

Fig. 5. Agreement between the mid-Holocene anomalies in LOVECLIM and in the proxies. Each marker type corresponds to a different proxy group. It is in green when the model agrees with the proxy record within the error bars; In blue, when the model agrees only with the sign of the anomaly; In red, when the model does not agree on the sign of the anomaly. If more than one proxy record is given at the same location, the markers representing the proxies are slightly shifted for improved readability.

CPD
9, 3953–3991, 2013

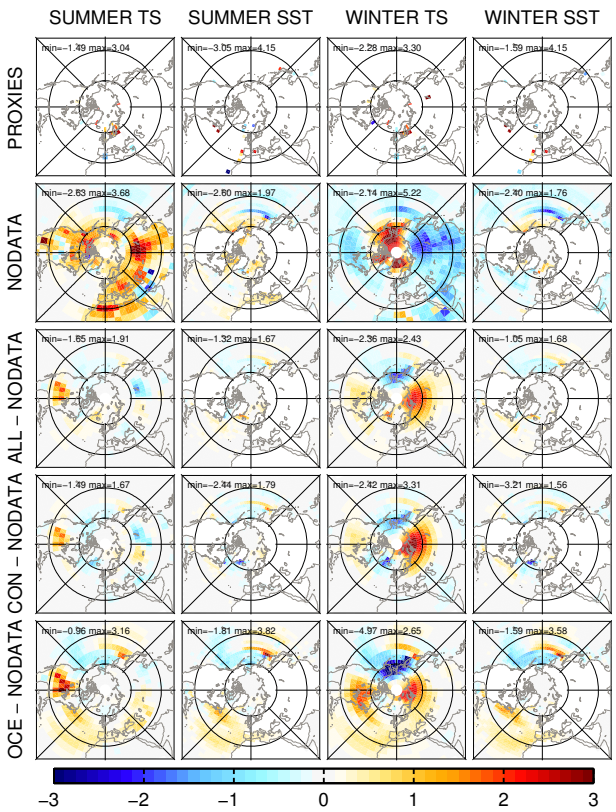

Fig. 6. Mid-Holocene air and sea surface temperature anomaly (˚C) for the proxies and the LOVECLIM simulation performed without data assimilation (NODATA). The reference period is 950 to 450 yr BP. Differences between the three simulations performed with data assimilation (ALL, CON and OCE) and the simulation NODATA (˚C). Winter corresponds to December to February (DJF) and summer to June to August (JJA).

CPD
9, 3953–3991, 2013

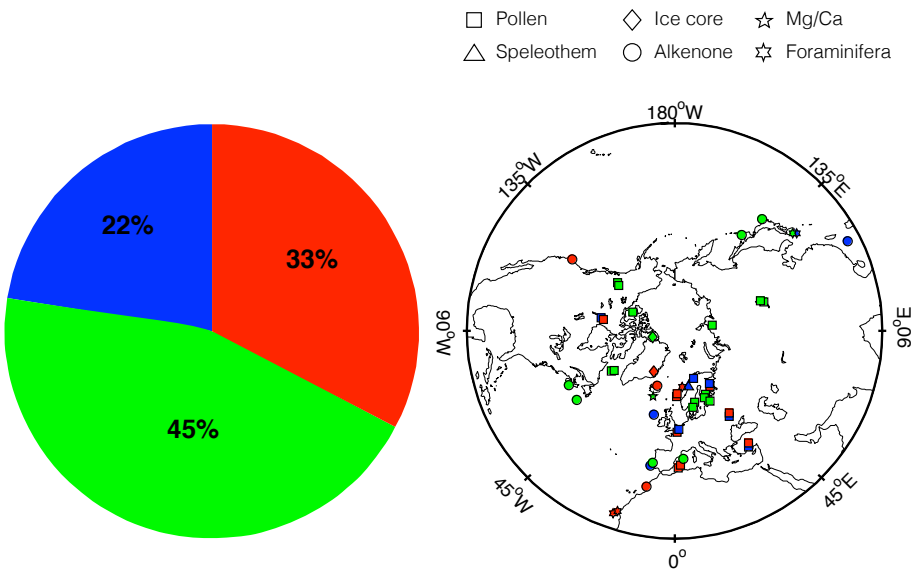

Fig. 7. Percentage and location of mid-Holocene proxies for which: (i) the modeled anomalies without data assimilation and in the three simulations with data assimilation are always within the estimated uncertainty of a particular proxy record (in blue); (ii) the modeled anomaly of at least one simulation with data assimilation is more consistent with the proxy record at the same location if it is assimilated and is not less consistent in the others simulations with data assimilation (in green); (iii) at least one of the three simulations with data assimilation is less consistent with the proxy records than the simulation without data assimilation or that no improvement is brought when they are assimilated (in red). On the map, if more than one proxy record is given at the same location, the markers representing the proxies are slightly shifted for improved readability. Each marker type corresponds to a different proxy group.

CPD
9, 3953–3991, 2013

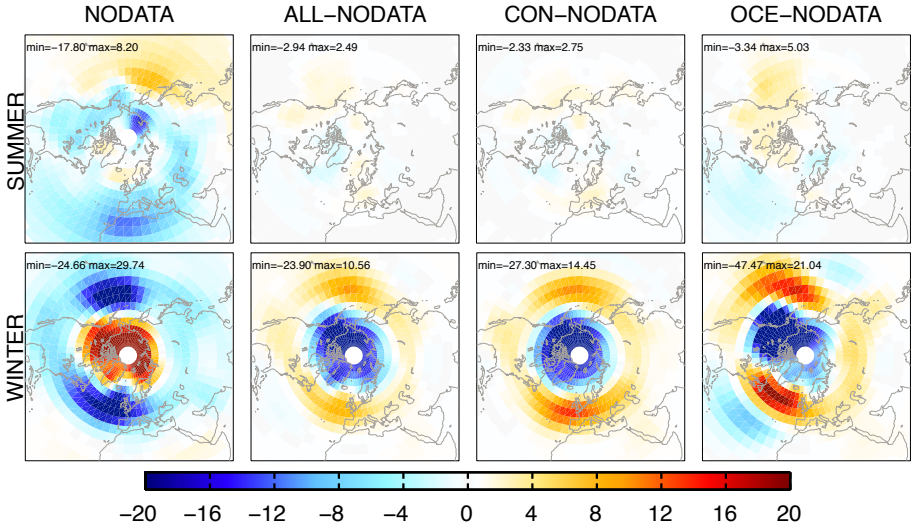

Fig. 8. Mid-Holocene geopotential height anomaly at 800 hPa (in m) for the simulation NODATA. The reference period is 950 to 450 yr BP. Difference between the three simulations performed with data assimilation (ALL, CON and OCE) and the simulation NODATA. Winter corresponds to December to February (DJF) and summer to June to August (JJA).

CPD
9, 3953–3991, 2013

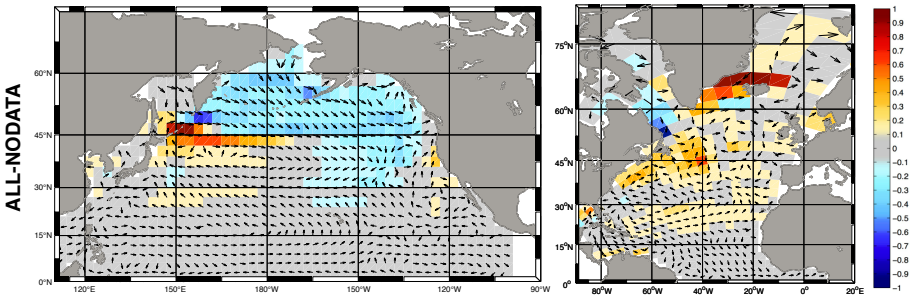

Fig. 9. Mean annual mid-Holocene difference of sea surface temperature (°C) and surface oceanic current for the Pacific and the Atlantic Ocean between the simulation ALL and the simulation NODATA. The size of the arrows is not proportional to their velocity to improve the readability of the maps since the objective is to show the current direction and not its strenght.

CPD
9, 3953–3991, 2013